Supplement of Biogeosciences, 21, 2877–2908, 2024
https://doi.org/10.5194/bg-21-2877-2024-supplement

Biogeosciences Open Access EGU

Supplement of

Disentangling influences of climate variability and lake-system evolution on climate proxies derived from isoprenoid and branched glycerol dialkyl glycerol tetraethers (GDGTs): the 250 kyr Lake Chala record

Allix J. Baxter et al.

Correspondence to: Allix J. Baxter (a.j.baxter@uu.nl) and Francien Peterse (f.peterse@uu.nl)

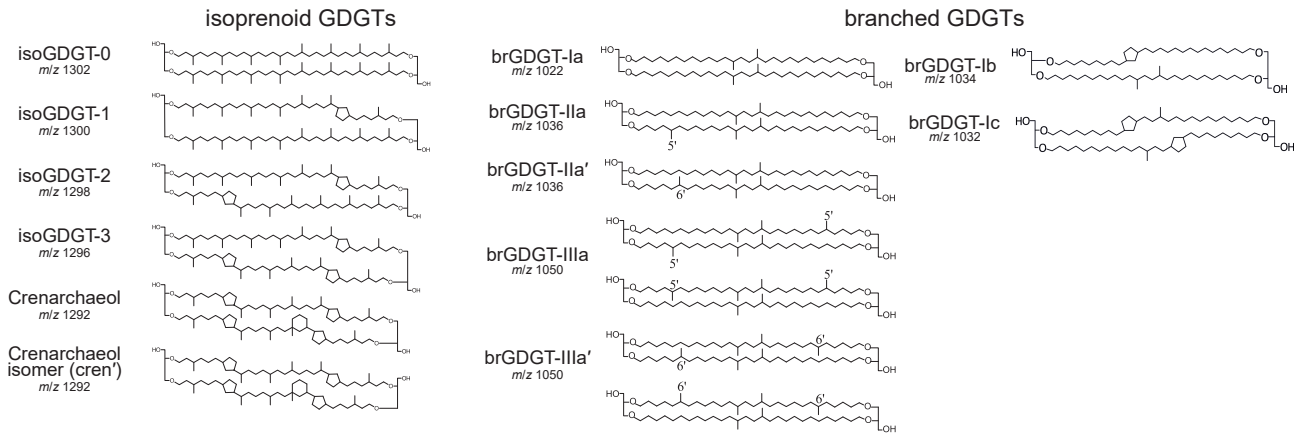

Figure S1. Molecular structure and names of iso- and brGDGTs used in GDGT indices and proxies presented in this study. BrGDGTs with one (as in IIa and IIa′) and two (as in IIIa and IIIa′) additional methyl groups may also include one or two rings (i.e., IIb-c, IIb-c′, IIIb-c and IIIb-c′; structures not shown).

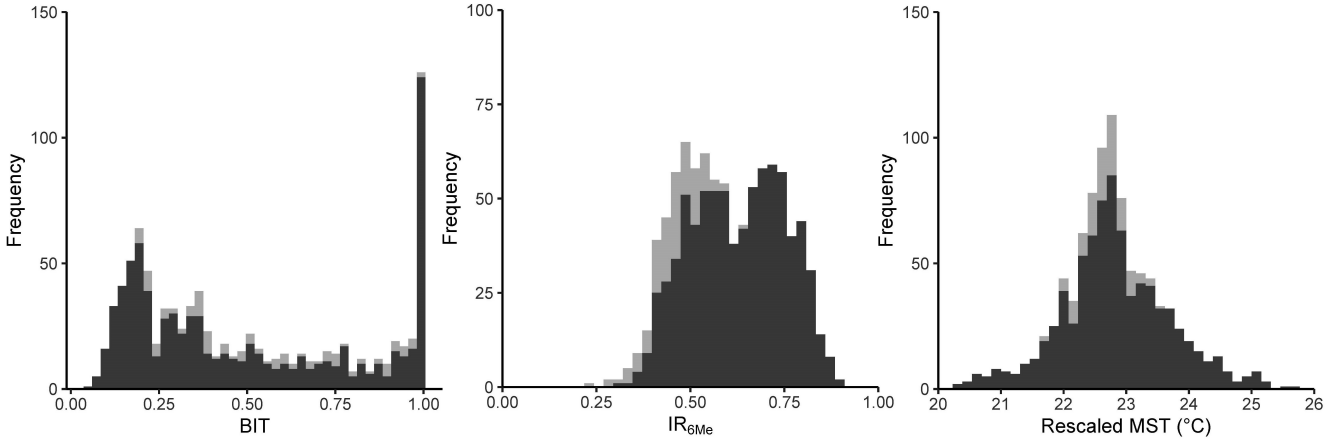

Figure S2. Frequency distribution of (a) BIT index (b) $\mathrm{IR_{6Me}}$ and (c) rescaled MST Pearson et al. (2011), Baxter et al. (2023) values throughout the 250-kyr DeepCHALLA sequence (grey) and in the section 180 - 0 ka (black).

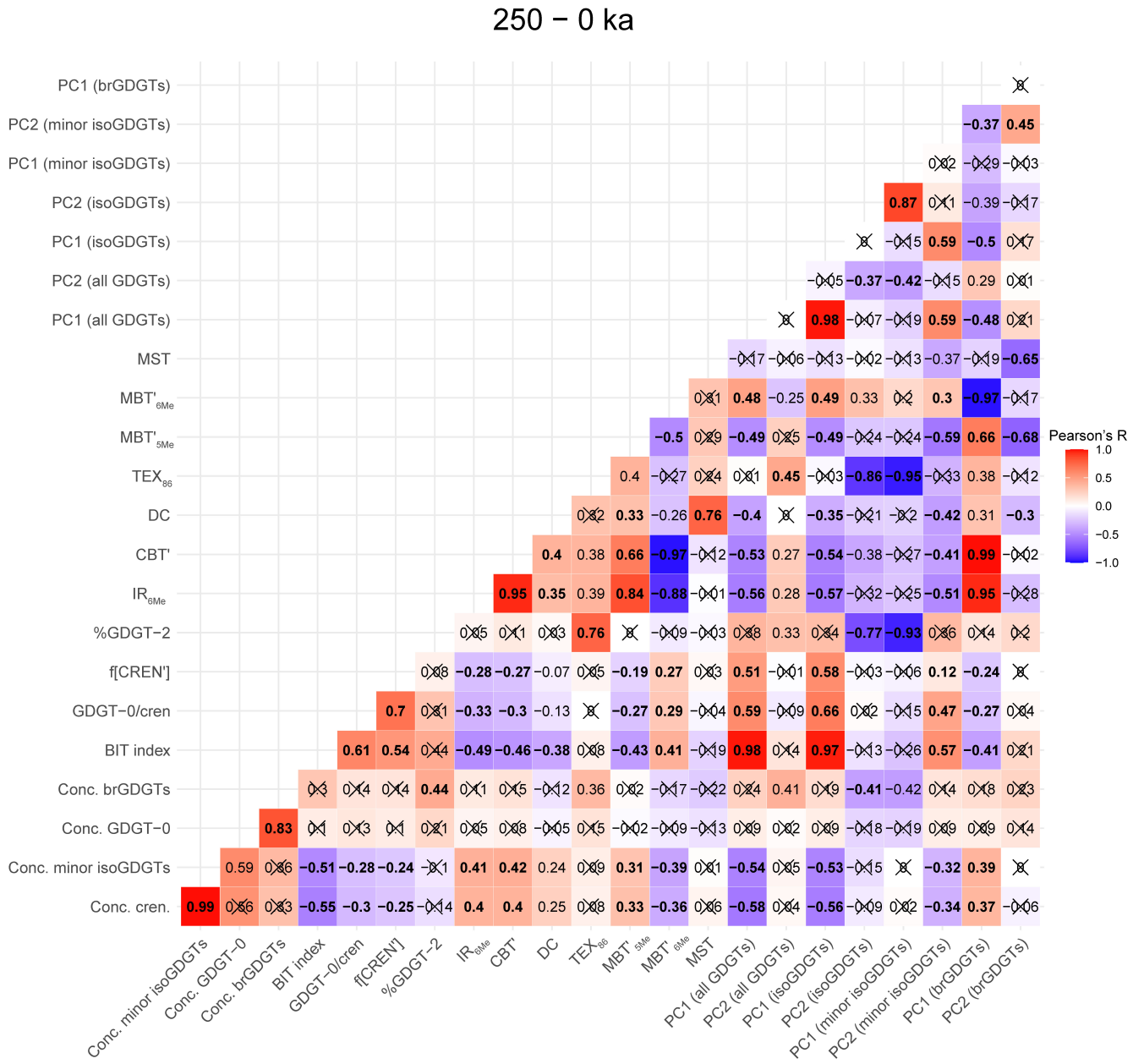

Figure S3. Pearson correlation (R value) matrix between time series of GDGT concentration, indices and principal component (PC) scores over the complete 250-kyr DeepCHALLA sequence (n = 906 samples with defined values for all variables). R values in bold are significant at $p < 0.001$, those in regular type at < 0.01, and those crossed out reflect lack of significance at the $p < 0.01$ level.

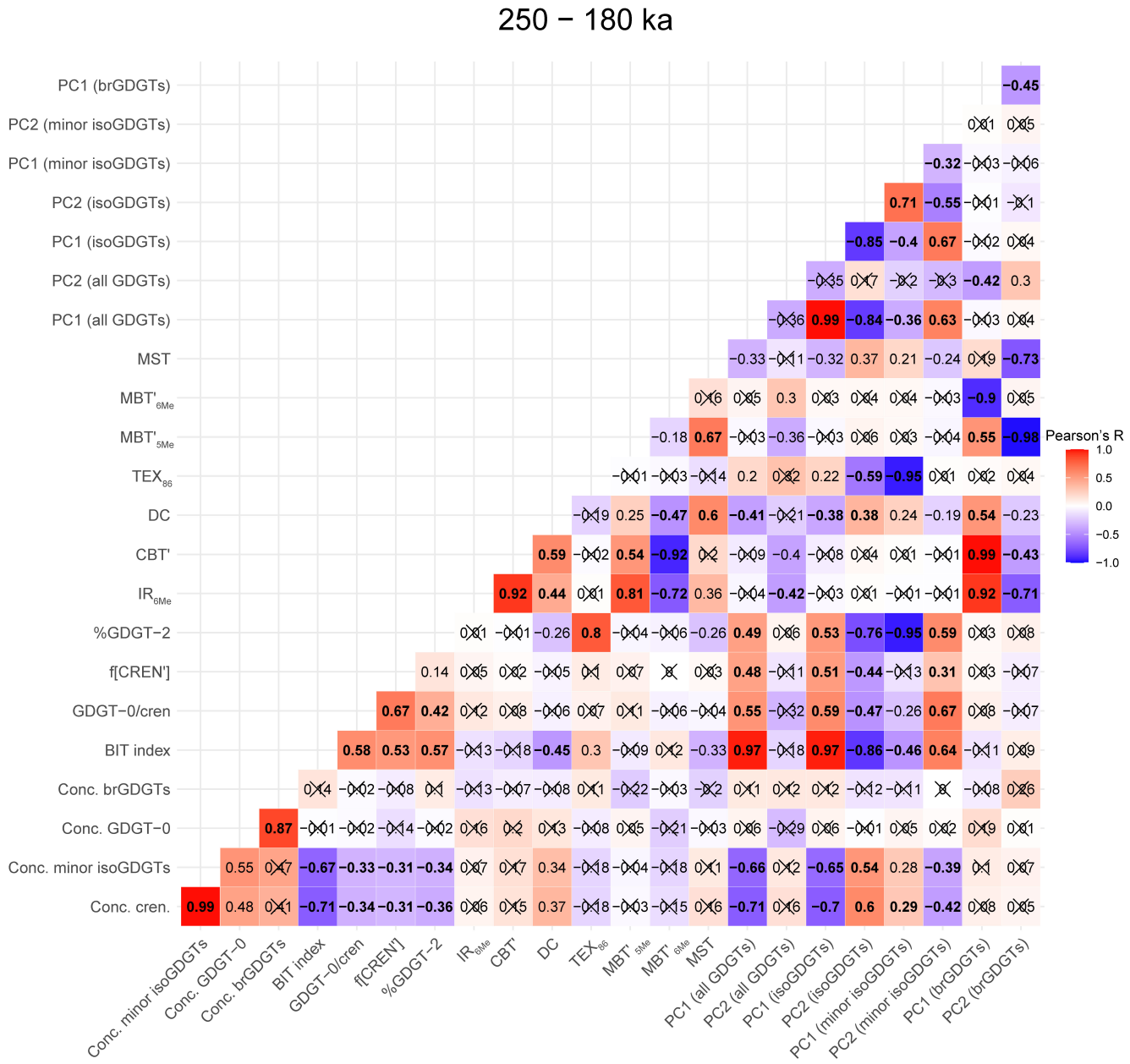

Figure S4. As Fig. S3 but for the period 250–180 ka only (n = 117).

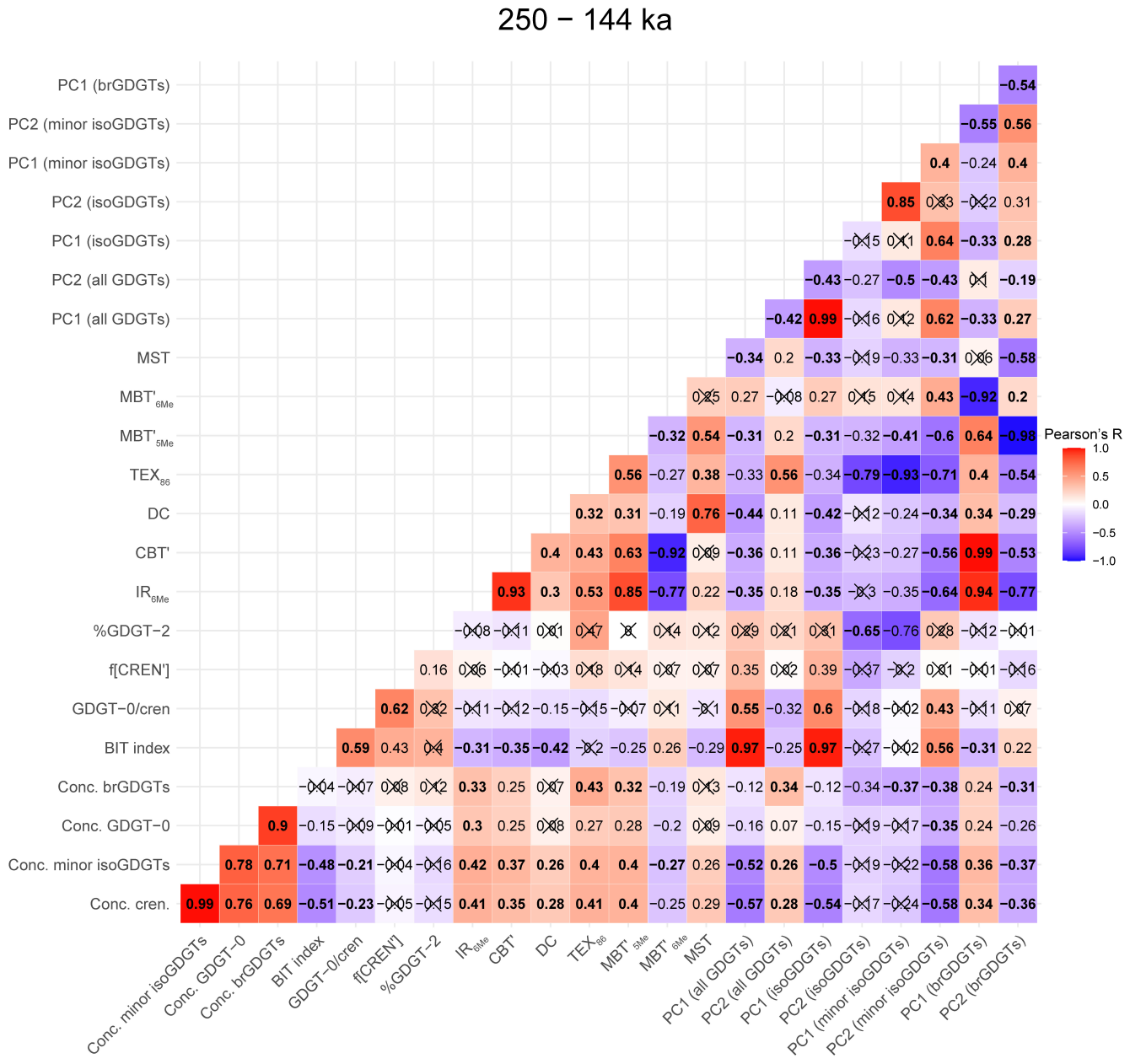

Figure S5. As Fig. S3 but for the period 250–144 ka only (n = 219).

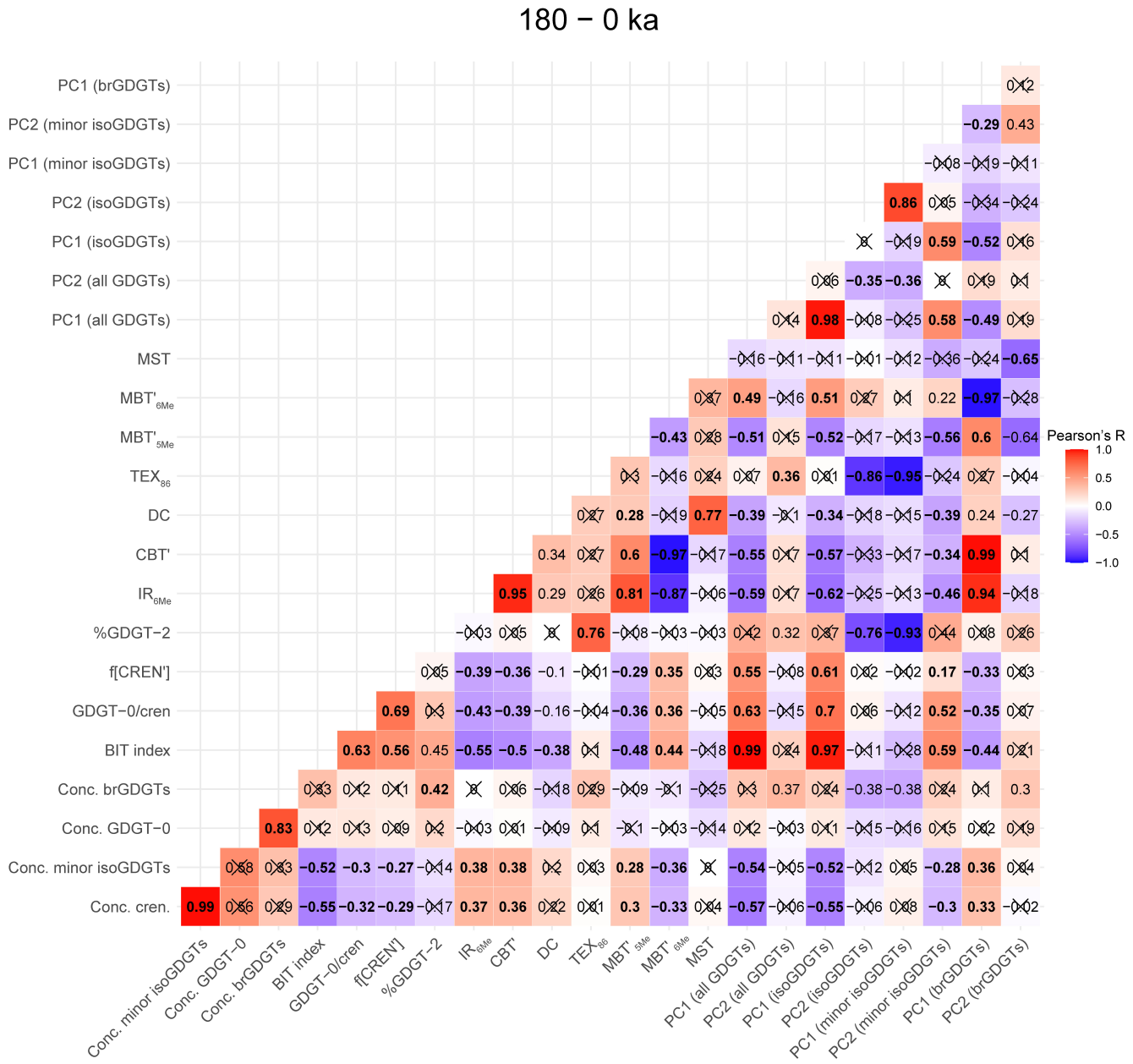

Figure S6. As Fig. S3 but for the period 180–0 ka only (n = 789).

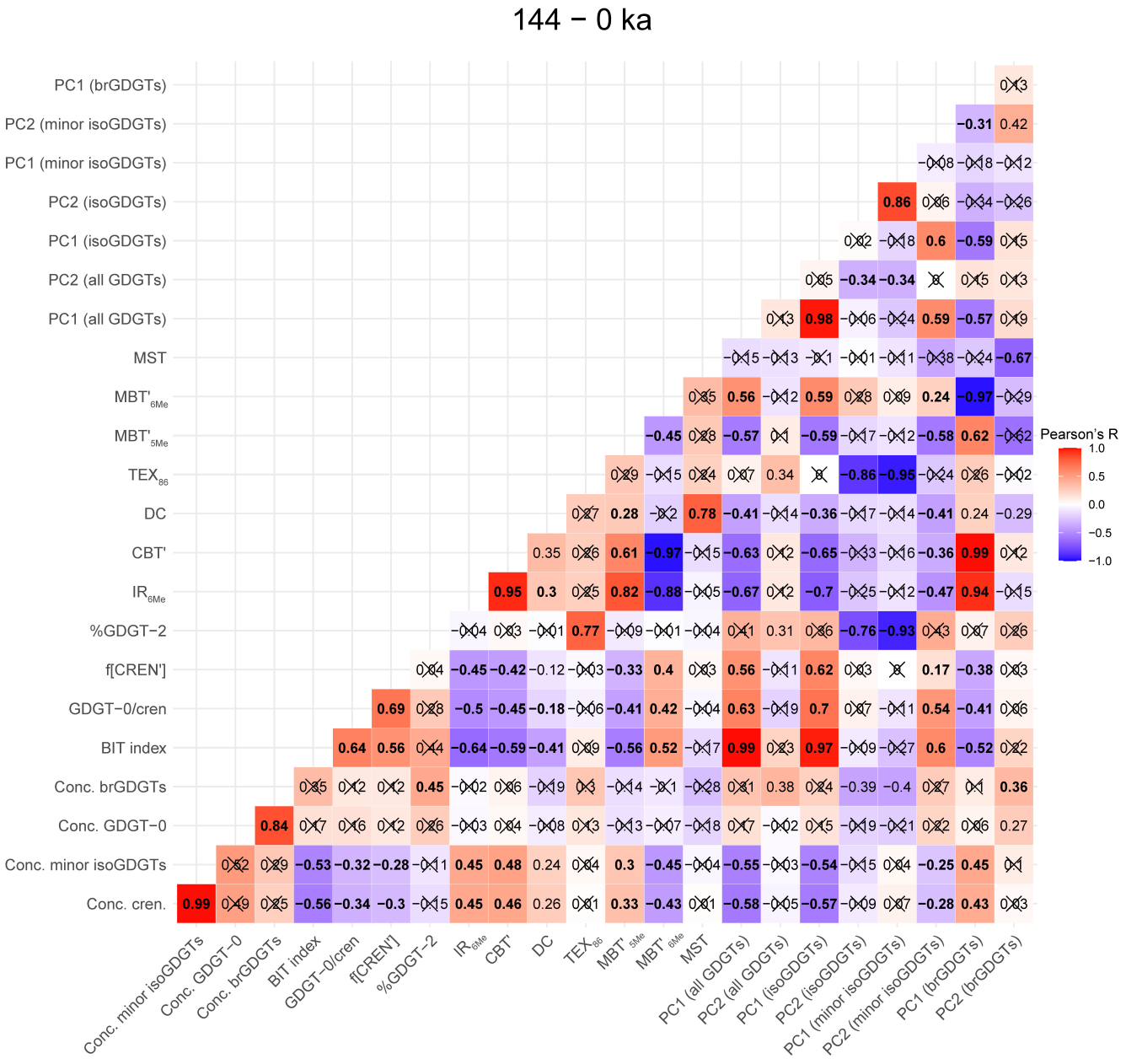

Figure S7. As described in Fig. S3 but for the period 144–0 ka only (*n*= 687).

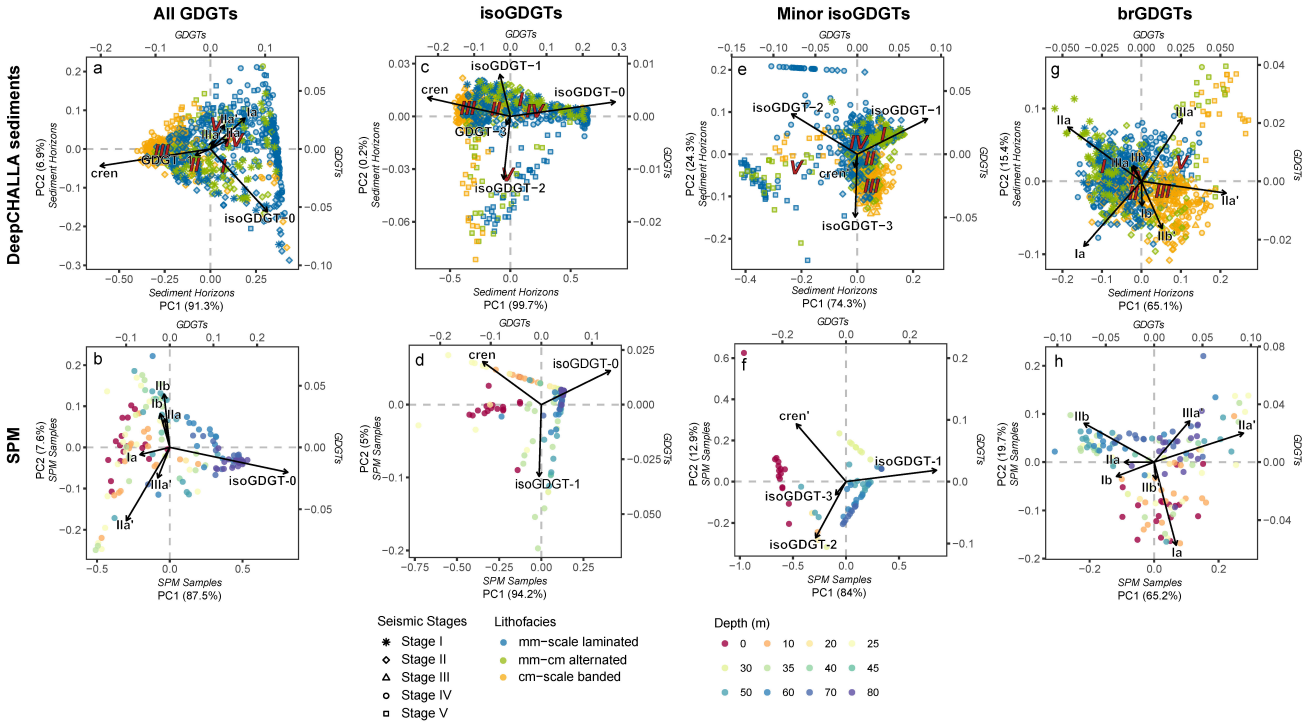

Figure S8. Principal component analysis (PCA) biplots of the fractional abundances of GDGTs in the DeepCHALLA sediment sequence and in suspended particulate matter (SPM) from modern-day Lake Chala. From left to right, biplots of all GDGTs in (a) DeepCHALLA sediments and (b) SPM, isoGDGTs in (c) DeepCHALLA sediments and (d) SPM, minor isoGDGTs (i.e., isoGDGT-1, -2, -3 and the crenarchaeol isomer) in (e) DeepCHALLA sediments and (f) SPM, and brGDGTs in (g) DeepCHALLA sediments and (h) SPM. Loadings of individual GDGTs contributing at least 1% to variability among samples on either PC1 or PC2 (or both) are shown as arrows. In the top panels, sediment horizons from depositional stages I-V are presented by different symbols, and colored according to lithofacies. Red numerals I-V represent the average PC scores of samples from those respective depositional stages. in the bottom panels, SPM samples are colored according to depth in the watrer column. Note the different scales of PC axes for individual samples (sediment horizons or SPM) and variables (GDGTs).

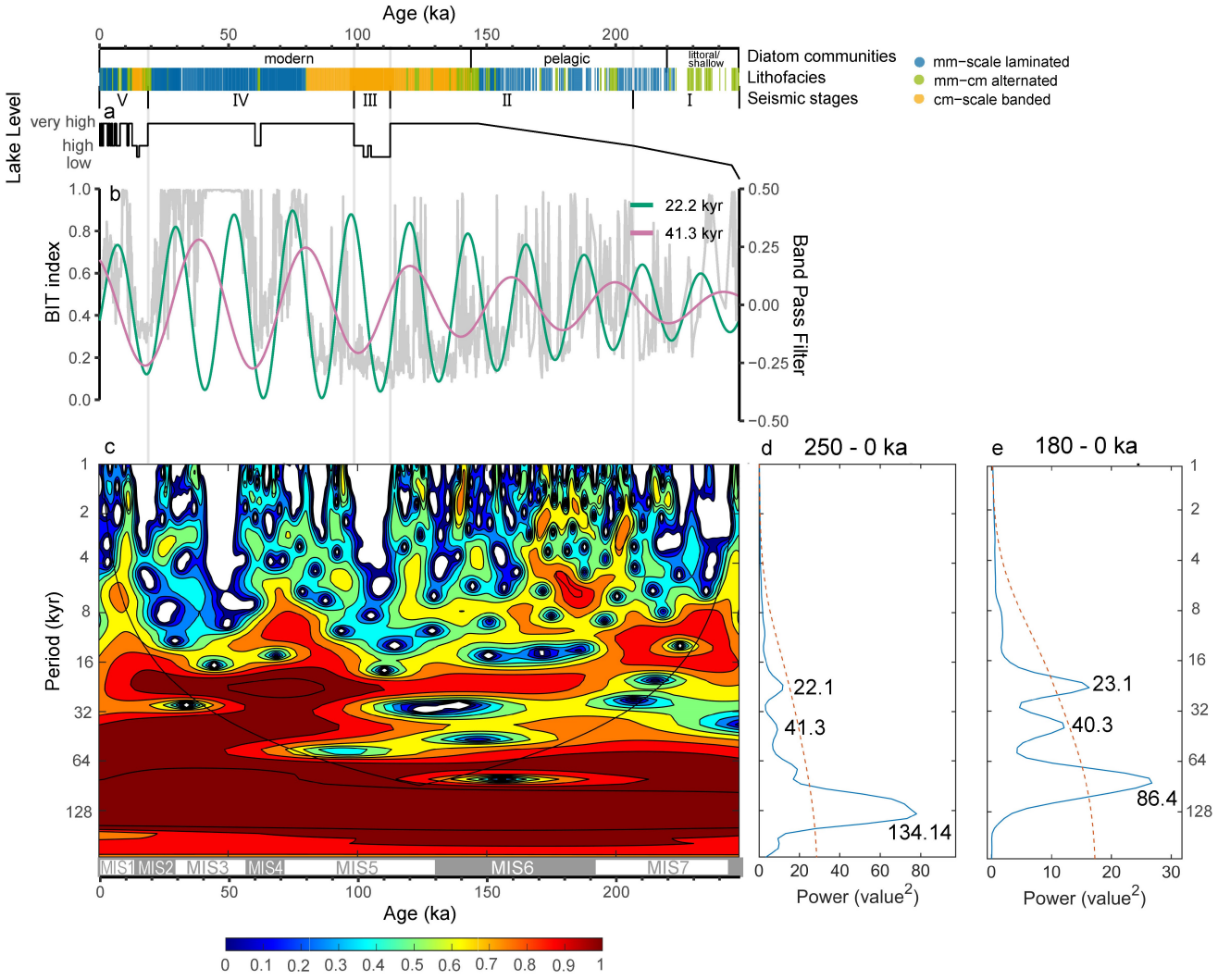

Figure S9. Periodicity analysis of the BIT index in the 250-kyr DeepCHALLA sediment sequence. Indicated on top are the timing of three major phases in lake ecology as registered in fossil diatom assemblages (Tanttu, 2021), the lithofacies category of each sediment horizon (colored bar) and the depositional stages (V-I) based on seismic stratigraphy Maitituerdi et al. (2022). Subsequent panels show (a) lake level reconstruction based on seismic stratigraphy (Maitituerdi et al., 2022), (b) the BIT index time series in light grey with green and pink curves representing the time series after band-pass filtering with periods similar to those of orbital precession and obliquity, as revealed by wavelet analysis, and (c) visual representation of wavelet analysis using a morlet function, with warm and cold colors reflecting high and low values of the power spectrum. Also shown is the timing of the marine isotope stages (MIS; Lisiecki and Raymo (2005)), for reference. Panels (d) and (e) summarize the BIT-index wavelet spectra in the complete DeepCHALLA sequence (250-0 ka) and in the section 180–0 ka only, to highlight more pronounced precession and obliquity cycles in the latter. The red stippled line in (d) and (e) represents the 95% confidence interval; dominant frequencies are labelled at the top of the maxima.

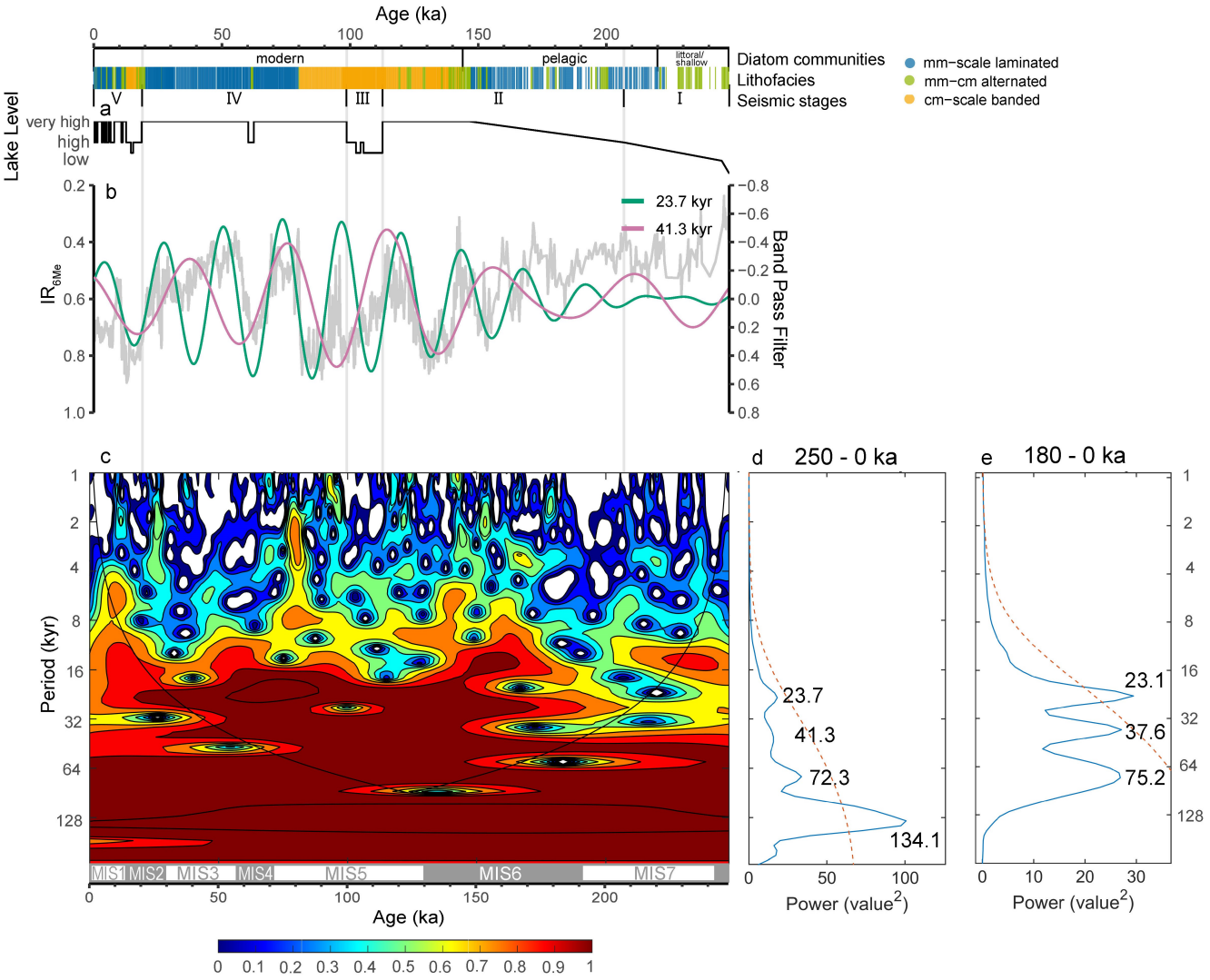

Figure S10. As Fig. S9 but for the ratio between 6-Me and 5-Me brGDGTs (IR_{6Me}).

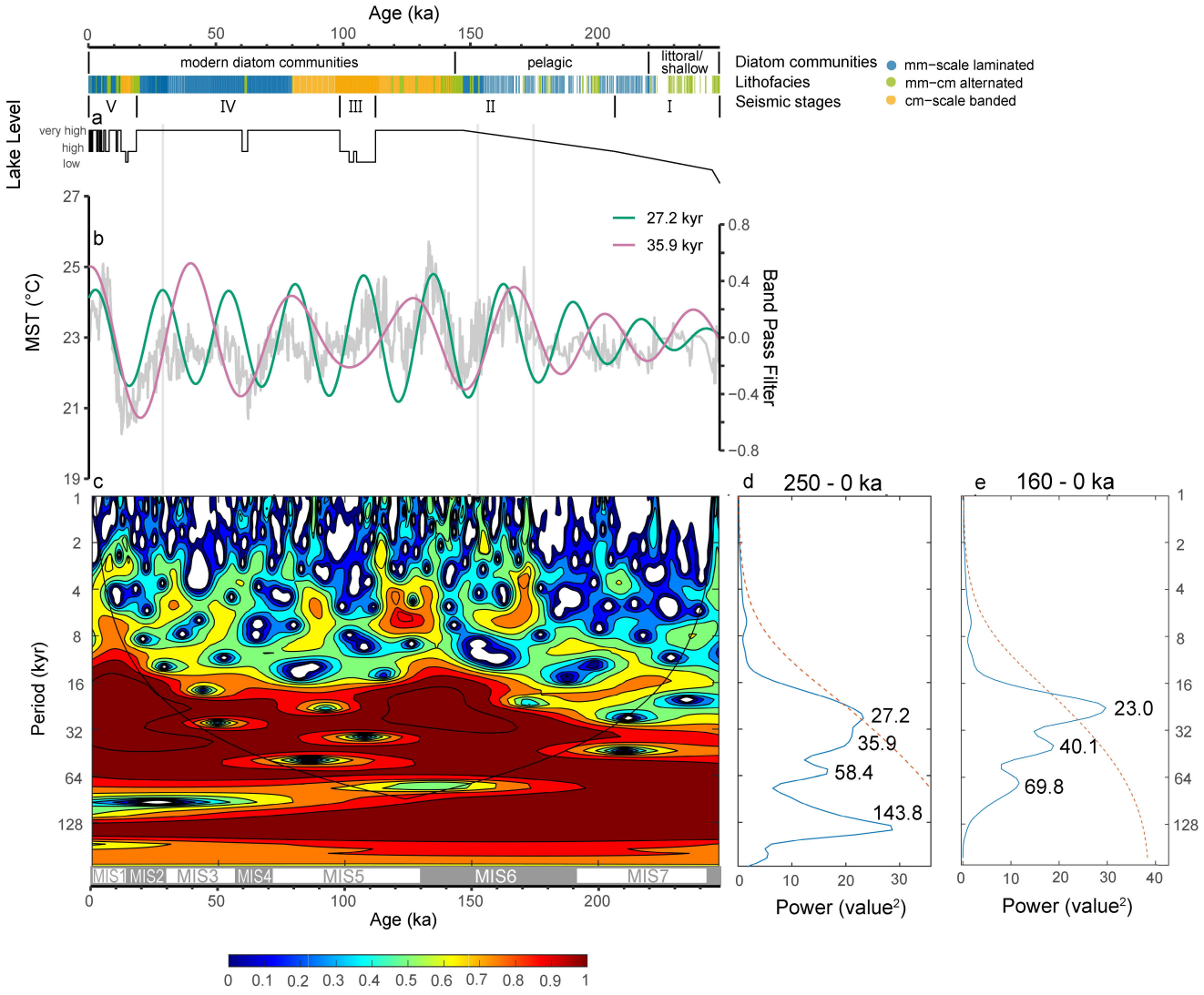

Figure S11. As Fig. S9 but for mean summer temperature (MST) reconstructed using the (Pearson et al., 2011) calibration of brGDGTs in globally distributed lake sediments, and with (e) representing the period 160 - 0 ka.

References

Baxter, A. J., Verschuren, D., Peterse, F., Miralles, D. G., Martin-Jones, C. M., Maitituerdi, A., Van der Meeren, T., Van Daele, M., Lane, C. S., Haug, G. H., Olago, D. O., and Sinninghe Damsté, J. S.: Reversed Holocene temperature–moisture relationship in the Horn of Africa, Nature, 620, 336–343, https://doi.org/10.1038/s41586-023-06272-5, 2023.

Lisiecki, L. E. and Raymo, M. E.: A Pliocene-Pleistocene stack of 57 globally distributed benthic δ 18O records, Paleoceanography, 20, https://doi.org/10.1029/2004PA001071, 2005.

Maitituerdi, A., Daele, M. V., Verschuren, D., Batist, M. D., and Waldmann, N.: Depositional history of Lake Chala (Mt. Kilimanjaro, equatorial East Africa) from high-resolution seismic stratigraphy, Journal of African Earth Sciences, 189, https://doi.org/10.1016/j.jafrearsci.2022.104499, 2022.

Pearson, E. J., Juggins, S., Talbot, H. M., Weckström, J., Rosén, P., Ryves, D. B., Roberts, S. J., and Schmidt, R.: A lacustrine GDGT-temperature calibration from the Scandinavian Arctic to Antarctic: Renewed potential for the application of GDGT-paleothermometry in lakes, Geochimica et Cosmochimica Acta, 75, 6225–6238, https://doi.org/10.1016/j.gca.2011.07.042, 2011.

Tanttu, H.: 250,000 years of diatom community dynamics in Lake Chala, a meromictic crater lake in equatorial East Africa, in: Past and present phytoplankton communities in East-African crater lakes: Paleolimnology and biomonitoring, unpublished Doctoral thesis, Ghent University, Belgium, 2021.